Aerodynamic modelling of fin stabilised underslung loads

K. Enciu
kobie@technion.ac.il

A. Rosen
aerosen@technion.ac.il

Technion – Israel Institute of Technology
Faculty of Aerospace Engineering
Haifa
Israel

ABSTRACT

Box-like slung loads exhibit periodic yaw response instabilities, while carried externally by a helicopter. When coupled with the slung load longitudinal and lateral pendulum motions, these instabilities result in significant pendulum oscillations of the load. High amplitude oscillations lead in many cases to the limiting of a load's flight envelope. Using wind tunnel and flight tests, rear mounted fins were previously demonstrated as efficient means for stabilisation of a problematic load. However, the lack of a proper analytical model of the stabilised load's aerodynamic characteristics, led to a trial and error development process, without an appropriate physical understanding of the stabilisation problem. The present paper describes a method for the aerodynamic modeling of fins stabilised slung loads based on a limited number of simple static wind-tunnel tests. The resulting database is incorporated in a dynamical slung load simulation that shows good agreement with dynamic wind-tunnel tests. The applicability of the proposed method is demonstrated, by the calculation of stabilised loads aerodynamic databases for interim fin inclination angles not covered by tests.

Paper No. 3991. Manuscript received 17 April 2014, revised version received 4 February 2015, accepted 19 March 2015.

https://doi.org/10.1017/S0001924000011143 Published online by Cambridge University Press

NOMENCLATURE

Acronyms

cg	centre of gravity
CFD	computational fluid dynamics
LCO	limit cycle oscillations
ac	aerodynamic centre
cp	centre of pressure

Symbols

$\underline{C}_{AER}$	vector of aerodynamic force and moment coefficients, expressed in load fixed co-ordinate system
C_D/C_{D0}	total/parasite drag coefficient
C_d	section (2D) drag coefficient
$\underline{C}_F$	vector of aerodynamic force coefficients, expressed in load fixed co-ordinate system
C_L	lift coefficient
C_{L_α}	flat plate section lift slope
C_l	flat plate section (2D) lift coefficient
C_M	pitch moment coefficient, expressed in wind co-ordinate system
$\underline{C}_M$	vector of aerodynamic moment coefficients, expressed in load fixed co-ordinate system
C_{Mx}, C_{My}, C_{Mz}	aerodynamic moment coefficients, expressed in fin fixed co-ordinate system
$C_{M_{c/4}}$	flat plate section pitch moment coefficient (referred to quarter chord), expressed in wind co-ordinate system
C_n	flat plate normal force coefficient
C_R	flat plate rolling moment coefficient, expressed in wind co-ordinate system
C_x,C_y,C_z	aerodynamic force coefficients, expressed in fin fixed co-ordinate system
C_Y	side force coefficient, expressed in wind co-ordinate system
D_A^B	transformation matrix from 'A' co-ordinate system to 'B' co-ordinate system
e	flat plate span efficiency factor (Oswald's efficiency factor)
$\underline{H}$	load angular momentum vector
$\underline{\underline{I}}$	load inertia tensor
i_F	fin inclination angle
g	gravity acceleration
K	lift induced drag factor
k	cross flow correction factor for the fin model
l_{REF}	load aerodynamic reference lengths
m	load mass
p	interpolation parameter
Pu_{av}	flat plate average upper surface pressure coefficient
q_∞	dynamic pressure
$\underline{r}$	load *cg* vector, measured from the centre of the gimbal system
S_{REF}	load aerodynamic reference areas
$\hat{\mathbf{x}}, \hat{\mathbf{y}}, \hat{\mathbf{z}}$	unit vectors in the longitudinal, lateral and vertical directions
x_{ac}	non dimensional fin chordwise aerodynamic centre

https://doi.org/10.1017/S0001924000011143 Published online by Cambridge University Press

x_{cp}, y_{cp} non dimensional fin chordwise and spanwise co-ordinates of centre of pressure
u, v, w flow velocity components in $\hat{x}$, $\hat{y}$, $\hat{z}$ directions
V_∞ incoming flow velocity

Greek symbols

α angle-of-attack
α_{S1}, α_{S2} angles-of-attack marking the start and end of stall transition region
β angle-of-sideslip
γ angle-of-drift
Δ change of aerodynamic property
ρ air density
$\underline{\omega}$ load angular rate vector
ψ, θ, ϕ load Euler angles (yaw, pitch and roll)

Subscripts and superscripts

$( )_F$ fin fixed co-ordinate system
$( )_L$ load fixed co-ordinate system
$( )_{XZ}$, $( )_{YZ}$ calculation based on velocity components in the corresponding plane
$( )_W$ wind co-ordinate system
$( )_{1/2}$ right fin/left fin

1.0 INTRODUCTION

External slung loads carriage by helicopters enables the aerial transportation of large and heavy loads, that cannot be carried internally. This allows the resupply of needed equipment to places where transport by land is impossible or limited by topographical, meteorological or other conditions. However, the maximum flight speed of the helicopter/slung load system is usually limited due to dynamic and aerodynamic instabilities. These instabilities, that are mainly affected by the load's aerodynamic characteristics, may significantly reduce the certified speed envelope for certain slung loads, thus leading to reduced operational efficiency and even increased risk to a helicopter crew operating in a hostile zone[1]. Loads prone to such instabilities include box-like loads (cargo containers), plate-like loads, different types of military loads (helicopter fuselages, trucks, bridge sections) and more. These 'difficult' loads were characterised by their respective geometrical and inertial properties, and classified into three groups[2] for the case of single point suspension.

In the case of box-like loads, the instabilities consist of a periodic yaw response that couples with the sling's longitudinal and lateral pendulum motions. These modes that were observed during isolated slung load dynamic wind-tunnel tests[3-6], are mainly the result of the unsteady aerodynamic attributes of boxes. Once attached to a helicopter, the coupling between helicopter and load modes creates complex response patterns, which affect the combined system's stability, handling qualities and ride quality.

Significant efforts have been made to date in modelling the aerodynamic characteristics of bluff bodies, in order to allow prediction by simulation of the combined helicopter/slung-load system's stability characteristics. Greenwell[7] provides a detailed review of these efforts, stating that they give no insight into the underlying flow physics, rely heavily on experimental data, and do not provide any means for prediction of new or modified load geometries. He then proceeds to

https://doi.org/10.1017/S0001924000011143 Published online by Cambridge University Press

present an alternative approach to static aerodynamic modelling of rectangular boxes. By introducing universal scaling rules, and using the velocities components parallel and perpendicular to each face, a method is developed that enables the prediction of aerodynamic coefficients for any rectangular box geometry.

Usage of CFD tools for the prediction of bluff bodies' static and dynamic aerodynamics can reduce the dependence on experimental test data, and provide a more accurate and flexible means for providing the aerodynamic data for a specific load. Theron *et al*[8] performed an unsteady flow analysis using CFD for the 6 x 6 x 8ft CONEX cargo container, and compared time averaged analysis results to static wind-tunnel test results. A follow on effort[9] involved analysis for a spinning CONEX, with its motion prescribed by the Euler angles time history from flight test data. Results indicated that CFD was accurate in reproducing the drag and the aerodynamic moments for both the stationary and spinning CONEX and insufficiently accurate in reproducing details of the lift and side force variations. The authors also noted that taking computational requirements into account, the current state of art in CFD was insufficient for engineering applications to cargo containers and other similar loads. Mantri *et al*[10] conducted a similar analysis for a static CONEX, and concluded that good agreement existed between CFD predictions and time-averaged side force and yawing moment measurements from dynamic wind-tunnel tests. Prosser & Smith[11] used CFD tools for development of a simple relation to predict the range of angles-of-attack where the lift remains approximately constant for semi-infinite rectangular bluff bodies. This prediction is useful for researchers attempting to develop simplified models of the forces acting on rectangular bluff bodies, since current 2D CFD tools are unable to provide adequate results in this angle-of-attack range.

Due to the speed envelope restrictions mentioned earlier, a key objective of slung load research is load stabilisation during forward flight. Several active and passive stabilisation techniques were examined in the past by various researchers[5,12-19]. These included the use of active jet, reaction wheels, variable geometry of the suspension system, the use of passive or active stabilisation fins, and more. However, none of these efforts matured into an operational system. A different approach to avoid slung load instabilities is the introduction of a flight director[20-23] that provides visual guidance to the pilot in damping the load pendulum modes and enables manoeuvering without their excitation.

In view of the load aerodynamics role in creation of slung load instabilities, one of the solutions to avoid or alleviate these phenomena is the modification of the load's aerodynamic characteristics by attachment of stabilising surfaces, either fixed (passive) or active. Raz *et al*[24] review past research related to the use of passive or active fins in stabilising slung loads, and mention that the design of such fins is not a simple task, owing to the need to establish the size, orientation and location of the fins. The effort described by these authors involved the development of fixed fins for stabilisation of a 8ft x 6ft x 6ft CONEX cargo container, currently limited to a maximum flight speed of 60kt when carried by a helicopter. Due to the inadequacy of existing simulations to predict slung load dynamics at medium and high flight speeds, the design process used dynamic wind-tunnel tests, and was basically that of a trial and error nature. Following these wind-tunnel tests, flight tests using a UH-60 Black Hawk utility helicopter were performed in order to confirm the agreement between wind-tunnel predictions and actual in-flight behaviour of the load, and thus prove the potential of using wind-tunnel tests as a tool in research of slung load stability.

The use of wind-tunnel tests in the certification process of slung load carriage enables a significant increase in safety, speed and cost effectiveness of this process when compared to relying uniquely on flight tests. Based on wind-tunnel test results, the required flight test scope can be significantly reduced to validation of the most critical configurations. However, as mentioned earlier, the determination of an optimal fin configuration is a complicated task that involves the need to

https://doi.org/10.1017/S0001924000011143 Published online by Cambridge University Press

determine various design parameters such as: fin shape, location, orientation, and number of fins. Furthermore, experience gained from wind-tunnel and flight tests[25] shows that load weight and centre of gravity (cg) offset play a significant role in the determination of a slung load's dynamic behaviour. Since it is impractical to study all the possible combinations of the various parameters that affect the system's dynamic stability through wind-tunnel tests, a verified numerical tool could prove very beneficial to the entire development and certification process. Such a tool is essential if better understanding of the complex nature of load dynamics is required, and very useful for the conduction of parameter sensitivity and tradeoffs analyses.

This paper describes the development of a quasi-steady aerodynamic model representing the two fins stabilised CONEX, which was used during the dynamic wind-tunnel tests and flight tests previously mentioned[24,25]. The initial modelling approach was based on accumulating the aerodynamic contributions of the net load and the isolated right and left rear-mounted fins. The resulting model would then be corrected for interference effects by using static wind-tunnel data of the stabilised load. During the development process it became clear that this approach of treating the stabilised load as a combination of isolated aerodynamic elements does not provide satisfactory results. Thus the model was revised so that the static aerodynamic properties of the stabilised load (fins included) are obtained from wind-tunnel tests, and a theoretical correction is applied in order to account for the fins increased aerodynamic damping due to the load's angular rates.

The paper starts in Section 2 with a description of the isolated fin aerodynamic model. This aerodynamic model is formulated to enable the prediction of the fin's aerodynamic coefficients for any combination of angles-of-attack and sideslip, and tuned to match static wind-tunnel test results for the isolated fin. Section 3 describes the static aerodynamic coefficients of the stabilised CONEX measured during static wind-tunnel tests. Assuming quasi-steady aerodynamics, the fins aerodynamic damping due to angular motions is evaluated using the isolated fin model that was presented in Section 2. This damping contribution is added to the stabilised load static aerodynamic coefficients to provide the complete aerodynamic model of the stabilised load. In Section 4, dynamic simulation predictions for the stabilised load are compared to dynamic wind-tunnel test results. It is demonstrated that the simulation is successful in predicting the system's dynamic behaviour, as observed during the dynamic wind-tunnel tests and flight tests. Section 5 demonstrates the validity of interpolating the aerodynamic database when wind-tunnel data for the stabilised load with interim fin angles are not available. Finally, the main conclusions from the research are summarised.

In the following sections the term 'load' will be used as reference to the net unstabilised load, and the term 'stabilised load' will be used to describe the load with two stabilisation fins attached to its rear corners.

2.0 ISOLATED FIN AERODYNAMIC MODEL

2.1 Fin description and model requirements

Figures 1 and 2 show the test helicopter carrying the fin stabilised CONEX cargo container, and a close-up of the left fin installation on the CONEX rear corner, respectively. Figure 3 presents the 1:11 scaled plywood model of the finned CONEX, used for the dynamic wind-tunnel tests described earlier[1,24,25]. The fin shape is close to being rectangular, with the upper half leading edge swept back 9° (see also Figs 4 and 5). The fin's cross section is also rectangular, with a thickness ratio of 4·3%. This implies that a flat plate aerodynamic model should be adequate for the description

https://doi.org/10.1017/S0001924000011143 Published online by Cambridge University Press



Figure 1. Test helicopter carrying the fins stabilised CONEX cargo container.



Figure 2. Rear-mounted left fin on CONEX container.



Figure 3. Stabilised CONEX model in the wind-tunnel.

of the static aerodynamic characteristics of the isolated fin. Fin inclination angle (referred to as 'fin angle' from here on), is defined as the angle between the load side face plane and the adjacent fin's plane, with the fin's trailing edge pointing outward. An important consideration is the wide range of angles-of-attack (α) and angles-of-sideslip (β) that the fins are subjected to during flight. When trimmed in flight, the load trail angle (the negative load pitch angle relative to the local vertical) might reach values as high as 50°. The fin inclination angles tested both in the wind-tunnel tests and in flight tests, were in the range of 20°-43°. This consideration alone shows that usually the fins do not operate in the linear lift region of a flat plate. When the velocities induced by the

https://doi.org/10.1017/S0001924000011143 Published online by Cambridge University Press

load's yaw, pitch and roll oscillations are included in the fins velocity calculation, the resulting fins angles-of-attack (α) could be well over ±90°. It is therefore clear that the aerodynamic model employed for the fins should be able to track the fins aerodynamic characteristics at this wide range of angles-of-attack and sideslip.

There are few models that meet this requirement. Ringland *et al*[26] developed a quasi-steady aerodynamic model for the prediction of the aerodynamic loads produced by an airship's tail on hull. The model assumes three different flow characteristics: a linear lift 'pre-stall' region for low angles-of-attack, a 'cross flow' region for high angles-of-attack, and a connecting 'stall transition' region in between. The fin's aerodynamic force components are calculated[26] using appropriately modified dynamic pressure expressions, rather than using the conventional dynamic pressure definition of $^1/_2\rho V_\infty^2$ (where ρ is the air density and V_∞ is the incoming flow velocity).

In order to check this model's suitability for the current research, slung load simulations were conducted employing it for predicting the fins aerodynamic loads. However, these resulted in an over prediction of the fins stabilising yaw moment as compared to existing flight test and dynamic wind-tunnel test data. Therefore, this model was not pursued further.

Another approach was suggested by Wick[27], who studied experimental and theoretical results for an inclined flat plate of infinite span. Results showed that thin airfoil theory is able to predict the lift generated by a flat plate at low angles-of-attack where the flow on the plate's upper surface is completely attached. However, at high angles-of-attack where the flow is completely detached as assumed by the Rayleigh-Kirchoff theory (discontinuous potential flow theory), the theory fails to provide a satisfactory prediction of the forces and moments on the plate due to established differences between the assumed and actual pressure distribution above the plate (the theory assumes that the flow wake above the plate is completely at rest rendering an average pressure coefficient equal to zero, whereas flow observations have shown that the fluid possesses definite vortical motion). Hence, it was suggested by the author to empirically modify the Rayleigh-Kirchoff theory by accounting for the differences between the theory predicted and the actual measured average pressure coefficient on the plate's upper surface, Pu_{av}. Wick's modified expressions for the force and moment coefficients of an infinite flat plate are:

$$C_n = \frac{2\pi \mathrm{Sin}\alpha}{4+\pi \mathrm{Sin}\alpha} - Pu_{av} \quad \ldots (1)$$

$$C_l = C_n \mathrm{Cos}\alpha \quad \ldots (2)$$

$$C_d = C_n \mathrm{Sin}\alpha \quad \ldots (3)$$

$$C_{m_{c/4}} = \frac{2\pi \mathrm{Sin}\alpha}{4+\pi \mathrm{Sin}\alpha}(0\cdot 25 - x_{cp}) + \frac{Pu_{av}}{4} \quad \ldots (4)$$

where the centre of pressure (*cp*) location in fractions of the plate's chord, measured from the leading edge, is:

$$x_{cp} = 0\cdot 5 - 0\cdot 75\frac{\mathrm{Cos}\alpha}{4+\pi \mathrm{Sin}\alpha} \quad \ldots (5)$$

It should be explained that the average upper surface pressure coefficient, Pu_{av}, is changing with

https://doi.org/10.1017/S0001924000011143 Published online by Cambridge University Press



Figure 4. Fin in wind-tunnel.

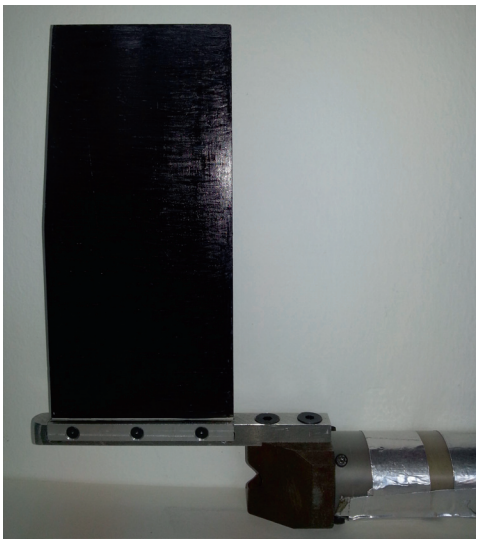


Figure 5. Fin and sting.

the plate's angle-of-attack. Using the modified expressions given above, a complete model for the calculation of forces and moments at an angle-of-attack range of 0°-90° was formulated. This model used thin aerofoil theory for low angles-of-attack (the 'pre-stall' region), a modified Rayleigh-Kirchoff theory (Equations (1)-(5)) for high angles-of-attack (the 'cross flow region'), and some sort of an interpolation for the region in between (the 'stall transition' region). It was decided that this model can form the basis for a detailed fin aerodynamic model to be used in the current research. However, certain adaptations and expansions must be made, if predictions of the aerodynamic surface's characteristics are required for the extended angles-of-attack and sideslip ranges of –90° to 90° and –180° to 180°, respectively. Another important key point is that the pressure coefficient correction term (Pu_{av}) can be established only through comparison between the theoretical model's predictions and supporting wind-tunnel test data or CFD analysis results. The specific structure of the model will enable the prediction of the aerodynamic characteristics of other fins similar in shape to the current one used. Such a prediction would combine thin wing theory for the low angles-of-attack range with a modification of Wick's model[27] for the high angle-of-attack range.

2.2 Isolated fin wind-tunnel test and model tuning

In order to provide information on the average upper plate's surface pressure coefficient as a function of angles-of-attack (α) and sideslip (β), a 1:10 tin sheet scale model of an isolated fin was tested in the Technion's open circuit low-speed wind-tunnel. The tunnel has a 1m x 1m test cross section, and can reach speeds over 80ms^{-1} with a uniformity of flow within 1% over this cross section (except for points very near to the tunnel walls). Figure 4 shows the fin installation in the tunnel, and Fig. 5 is a close up of the fin and the connection to the sting balance. The fin was first tested 'leading edge on' in order to provide measurements for the sideslip angle range of –90° to 90°, and then re-installed and tested 'trailing edge on' to provide measurements for the case of the flow incoming from the fin's trailing edge, where $90° < |\beta| < 180°$.

https://doi.org/10.1017/S0001924000011143 Published online by Cambridge University Press

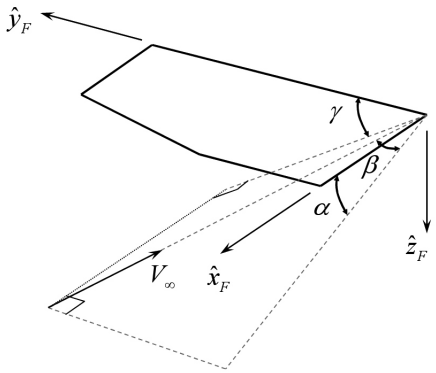
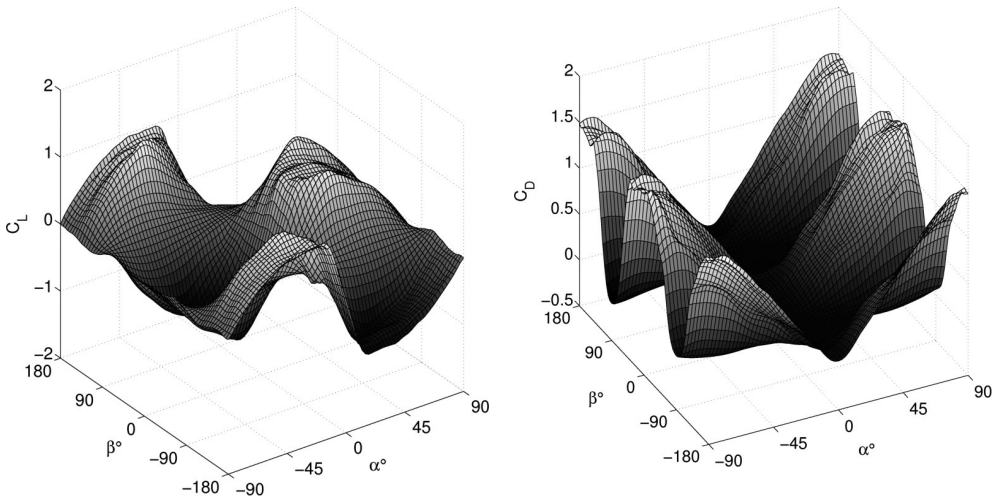


Figure 6. Definition of fin aerodynamic angles and body axes.



(a) Lift coefficient map (b) Drag coefficient map

Figure 7. Fin lift and drag coefficients map.

Angle-of-attack and sideslip angle definitions are consistent with the regular convention of wind axes to body axes transformations (the reader is referred to Fig. 6 for the definition of these angles). The test balance and fin holder were also tested without the fin installed, in order to allow correction of the measured results for the balance and holder aerodynamic contributions, to receive the net fin's forces and moments. Figures 7(a) and 7(b) show the results for the lift and drag coefficients map respectively, as functions of α and β.

The isolated fin tuning was achieved in two stages: in the first stage, the fin's 3D linear lift slope (C_{L_α}), parasite drag coefficient (C_{D0}), span efficiency factor (e) and chordwise aerodynamic centre (x_{ac}) were established using the linear lift region of the angle-of-attack sweep data for 0° sideslip angle. Once the fin's 'linear lift' model coefficients were established, the second stage of tuning the upper surface pressure coefficient was performed. For this stage, a modified set of equations was used in place of the original Equations (1), (4) and (5) of Wick's model[27]. Since the original

https://doi.org/10.1017/S0001924000011143 Published online by Cambridge University Press

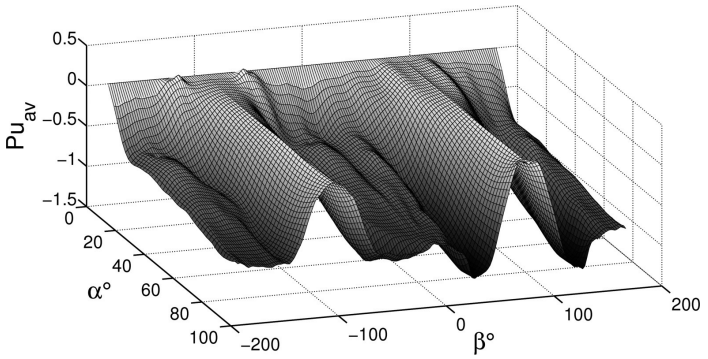


Figure 8: Tuned upper surface pressure map.

model was derived assuming an infinite span plate (without tip effects), a factor k was introduced in the modified model to account for the 3D end effects. These are expected to reduce the cross flow term's magnitude due to the roll up of the fin's tip vortex, increase the average pressure on the upper surface and thereby reduce the normal force coefficient[28]. In addition, the modified equations use the tuned value of the fin's aerodynamic centre (ac) for the linear lift region, in place of the theoretical value of 0·25 in Equations (4),(5). The modified model is formulated in Equations (6)-(8):

$$C_n = \frac{2\pi k \mathrm{Sin}\alpha}{4+\pi \mathrm{Sin}\alpha} - Pu_{av} \quad \ldots (6)$$

$$C_{mac} = \frac{2\pi k \mathrm{Sin}\alpha}{4+\pi \mathrm{Sin}\alpha}(x_{ac} - x_{cp}) + Pu_{av}(0\cdot 5 - x_{ac}) \quad \ldots (7)$$

$$x_{cp} = 0\cdot 50 - (2 - 4x_{ac})\frac{\mathrm{Cos}\alpha}{4+\pi \mathrm{Sin}\alpha} \quad \ldots (8)$$

The upper surface average pressure coefficient, Pu_{av}, is extracted for every test point using equation (6) of the revised normal force coefficient[6]. Alternatively one may consider using the lift or drag coefficients for the extraction of the pressure coefficient. However, analysis shows that these lead to acceptable model predictions for only a portion of the required angle-of-attack range[29].

Up to this point, the development of the fin's model included only the data set for a zero sideslip angle. The main assumptions and basic model predictions were laid out in consideration of this dataset alone. However, if the complete model should be able to predict the aerodynamic coefficients for any required value of sideslip angle, it is obvious that this parameter should be incorporated in the model as well. In order to achieve this goal, the normal force coefficient of Equation (6) is expanded to also include dependency on the fin's sideslip angle. The average upper surface pressure coefficient, Pu_{av} , thus becomes a function of both angles-of-attack and sideslips, and is extracted from wind-tunnel test results using the expanded model for the normal force coefficient[29].

Figure 8 presents a carpet plot of the resulting upper pressure map as a function of angles-of-attack and sideslip. The results were treated[30] to reflect symmetry with respect to angle-of-attack, as anticipated for an ideal flat plate or a zero camber airfoil wing. The same cannot be said for

https://doi.org/10.1017/S0001924000011143 Published online by Cambridge University Press

the sideslip angle. Results clearly show that the average upper surface pressure coefficient values are asymmetric with respect to the sideslip angle. This is expected due to the fin shape not being symmetric spanwise, and because of the fin and balance interference effects.

As explained earlier, net fin loads were obtained from the test results by subtracting the holder and balance aerodynamic loads from the fin plus balance measurements. It was observed from the wind-tunnel test results for fin sideslip angles close to ±90° that the test balance and holder create a significant aerodynamic interference that alters the flow pattern over the fin for this sideslip angle range. Tare measurements for the balance and holder showed that for low α, and with β close to ±90°, the extracted data for net fin forces and moments was of dubious quality. For these (α,β) combinations, one or more components of the net balance force aerodynamic coefficients had the same order of magnitude as those of the fin plus balance. Therefore, it was understood that the measurements for this angle range were distorted to a large extent. For this reason, for the low angle-of-attack/high sideslip angle combinations, net balance measurements were not subtracted from the total fin plus balance measurements to produce net fin forces and moments, as opposed for the procedure followed for most of the angles-of-attack and sideslip range. It should be emphasised that this particular angle range is unimportant for the current research, as it was never encountered in dynamic simulations.

2.3 Fin aerodynamic forces and moments

Once the upper surface pressure correction terms were obtained, the complete aerodynamic model for the isolated fin could next be defined. The model follows Ringland *et al*[26] by assuming that the aerodynamic moments and in plane forces (drag and side force) are dependent on modified dynamic pressures that do not include the corresponding lateral velocity component. Thus, the axial force and pitch moment are calculated using the expression $\frac{1}{2}\rho\sqrt{u^2+w^2}$ for the dynamic pressure, and the side force and roll moment are calculated using $\frac{1}{2}\rho\sqrt{v^2+w^2}$. The fin's aerodynamic forces and moments coefficients are first calculated by using the angle-of-attack α and drift angle γ, for determination of the appropriate flow region model to be used (i.e. linear, cross flow, or interpolation between the two). Using the modified expressions for the dynamic pressures, the fin's aerodynamic force and moment components are then calculated. The fin aerodynamic model formulation is presented in Appendix A.

The resulting net fin aerodynamic database is demonstrated in Figs 9(a-d) and 10(a-d) showing a comparison between model predictions and wind-tunnel test results for sideslip angles of 0° and 60°, respectively. The results, which are plotted in wind axes, show that the main purpose of adequate prediction of the principal fin force coefficients (namely lift and drag), is achieved. Also shown is the fin normal force coefficient (in fin axes), which demonstrates the successful tuning of the model's predictions to test results. It is shown that the predicted normal force coefficient closely follows the test data in the whole angle-of-attack range. The differences in Figs 10(a) and 10(b) between test and prediction in the in plane force coefficients (drag and side force) for low angles-of-attack are due to the obvious shrinking of the linear lift region as the sideslip angle is increasing. This effect that is currently not included in the model, could be easily implemented if required, by introducing a change of the stall transition region (through the parameters α_{S1} and α_{S2} as a function of sideslip angle). Another observation from Fig. 9 is that unlike the assumption of zero side force coefficient for zero angle-of-attack, actual test measurement values are different from zero, although generally very small.

https://doi.org/10.1017/S0001924000011143 Published online by Cambridge University Press

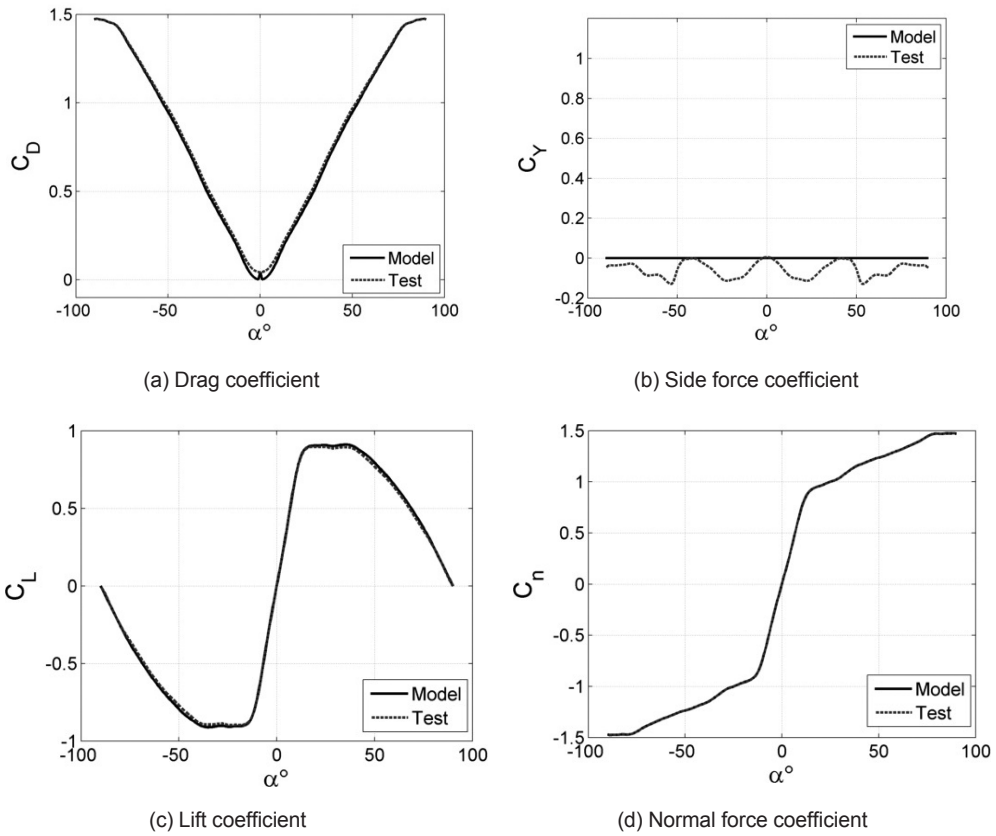


Figure 9. Fin aerodynamic coefficients, sideslip angle = 0°.

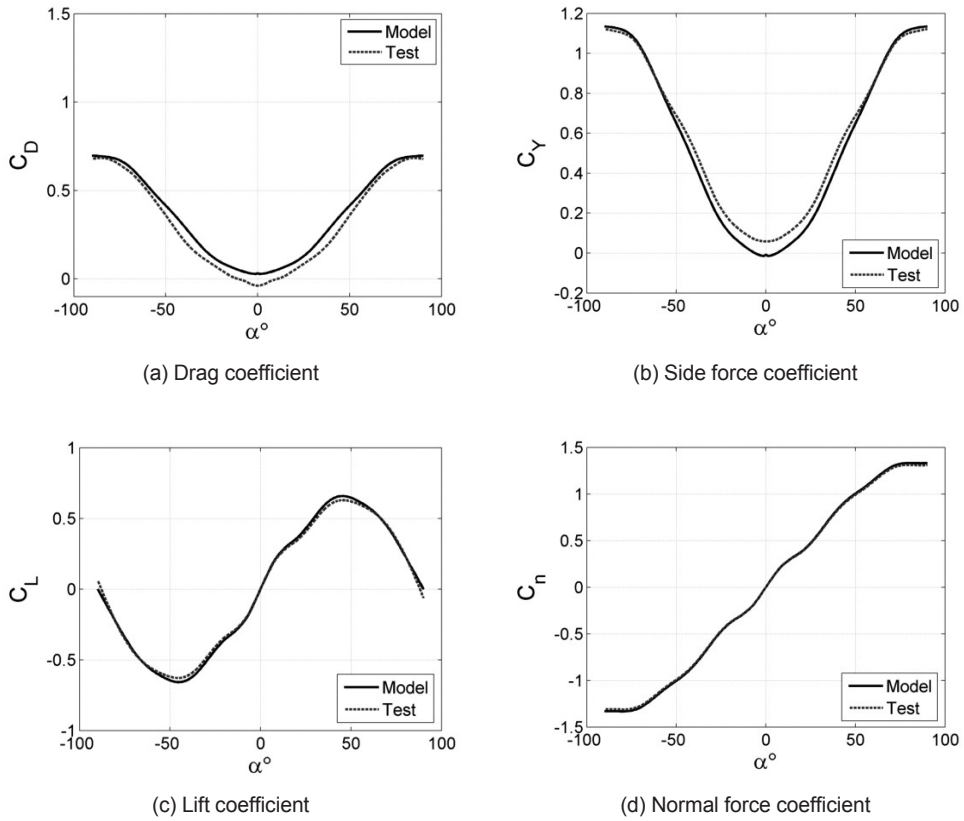
Comparisons between the predicted and measured pitch, roll and yaw moment coefficients were also made[29]. These showed that pitch and roll moment coefficients were under predicted, a possible indication that the fin's *cp* in the cross flow region is located further aft than what is assumed by the model. In addition, the assumption that the fin's roll moment coefficient (C_R) is equal to zero increased the inaccuracy of moment predictions for sideslip angles different than zero. Measured values different from zero were obtained for the fin yaw moment. This is due to the fin and balance interface, and the spanwise shift of the fin's centre of pressure with changing angles-of-attack and sideslip. The effect of all the above inaccuracies of the model become secondary to negligible, once fin aerodynamic characteristics are combined with those of the net slung load to provide the stabilised load aerodynamic database.

3.0 STABILISED CONEX AERODYNAMIC MODEL

3.1 Wind-tunnel test description

The flow pattern expected near the load rear face is different from the undisturbed free stream velocity that existed during the isolated fin wind-tunnel tests, due to various effects such as: load boundary layer, flow separation on load faces, load rear face wake, and more. These cause

https://doi.org/10.1017/S0001924000011143 Published online by Cambridge University Press



(a) Drag coefficient (b) Side force coefficient

(c) Lift coefficient (d) Normal force coefficient

Figure 10. Fin aerodynamic coefficients, sideslip angle = 60°.

significant changes in the local flow at the rear of the load, near the fins attachment points. Therefore, the dynamic pressure and local flow direction in this area are altered in comparison to the free stream undisturbed flow. It follows, that any attempt to theoretically predict the fins aerodynamic forces and moments when mounted on the rear part of the load must account for these interference effects.

It can be assumed that the aerodynamic contribution of specific fins when attached to different slung loads, can be estimated based on similarity considerations between the geometric shapes of these loads. Following this assumption, it is suggested to consider a stabilised load aerodynamic coefficients vector, $\bar{C}_{AER}$, as being composed of the sum of the net load's aerodynamic coefficients vector, $(\bar{C}_{AER})_{LOAD}$, and the fins aerodynamic contribution vector (including load/fins interference effects), $\Delta\bar{C}_{AER}$. The latter can easily be determined from wind-tunnel test data by subtraction of the net load test data from the stabilised load test data:

$$\Delta\bar{C}_{AER} = (\bar{C}_{AER})_{LOAD+FINS} - (\bar{C}_{AER})_{LOAD} \quad \ldots (9)$$

To this end, a two stage static wind-tunnel test has been conducted. In the first stage, the CONEX cargo container 1:11 scale plywood model used earlier for dynamic wind-tunnel tests[24,25] was mounted in the Technion low-speed wind-tunnel, and its aerodynamic properties measured. In the second stage, model fins were added, and the wind-tunnel test was repeated. Fin inclination

https://doi.org/10.1017/S0001924000011143 Published online by Cambridge University Press

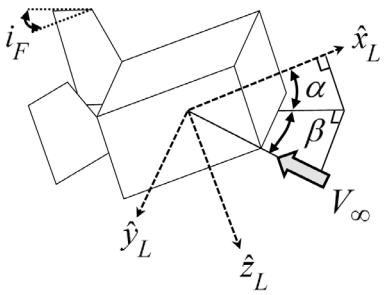
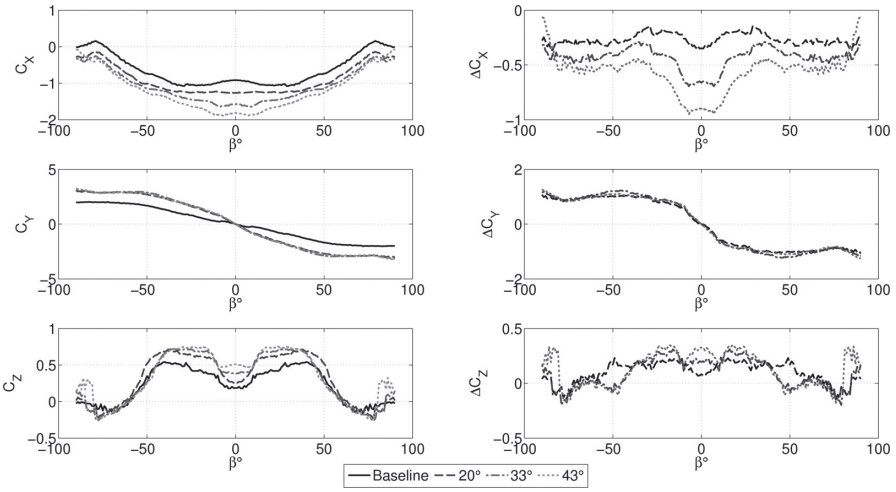
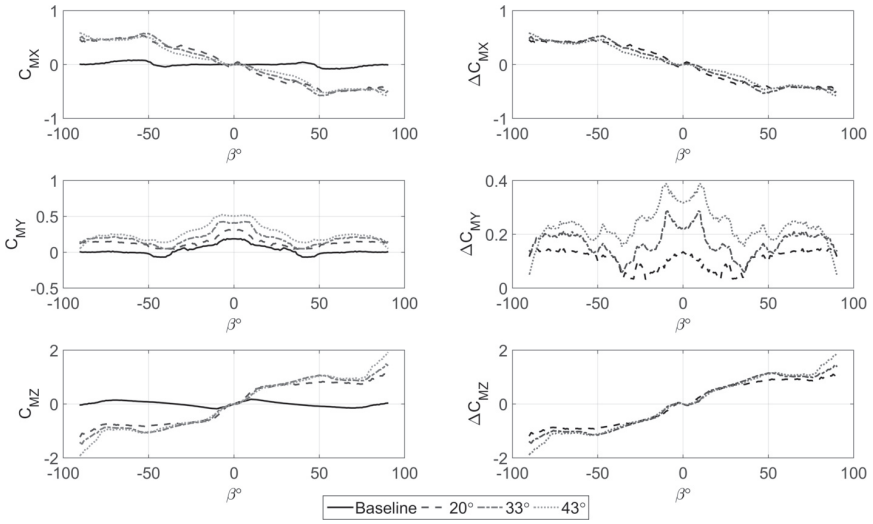


Figure 11. Definition of load aerodynamic angles and body axes.



(a) Aerodynamic force coefficients.



(b) Aerodynamic moment coefficients.

Figure 12. Stabilised load aerodynamic coefficients for three fin angles (20°, 33° & 43°), angle-of-attack = –10°.

https://doi.org/10.1017/S0001924000011143 Published online by Cambridge University Press

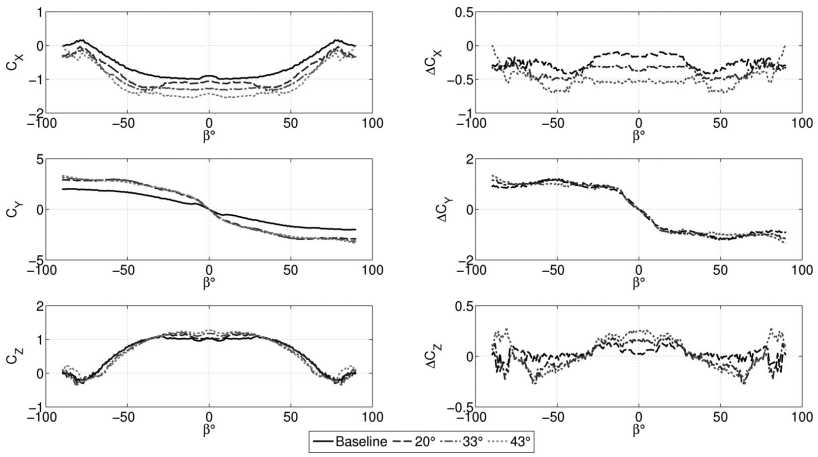
angles were set at 20°, 33° and 43°, to allow the preparation of aerodynamic databases representative of the stabilised CONEX configurations, for which both dynamic wind-tunnel tests and flight test data are available[24,25]. The CONEX model used for the tests did not include the full scale CONEX face details (corrugated walls and forklift holes), as these were reported by Rosen *et al*[30] to have a relatively small effect on the measurements for most of the available test data. The reference point for the moments measurements was set at the net load's geometric centre. The current wind-tunnel test included sideslip angle sweeps of –90° to 90° in constant angles-of-attack. The reader is referred to Fig. 11 for the definitions of angles-of-attack, sideslip and fin inclination (i_F) for the load wind-tunnel test.

Angle-of-attack test points for sideslip angle sweeps were changed from –70° to 70° in 5° increments, but data used for post-test analysis excluded angles-of-attack above 60° and below –60° due to the strong load/balance interference at these angles. Angles-of-attack and sideslip test ranges were determined such that flow conditions during stabilised slung load operations would be mapped, thereby eliminating the need to test for sideslip angles larger than ±90°. It should be explained that the stabilised load aerodynamic database was treated to reflect the expected symmetry and anti-symmetry with respect to sideslip angle. The database for the net load, which has the geometric form of a rectangular box, was originally treated[30] for symmetry and anti-symmetry with respect to the angles-of-attack and sideslip. Test points for the net load were taken only for positive angles-of-attack, and then symmetry and imaging rules were used for extraction of a complete aerodynamic database for the CONEX.

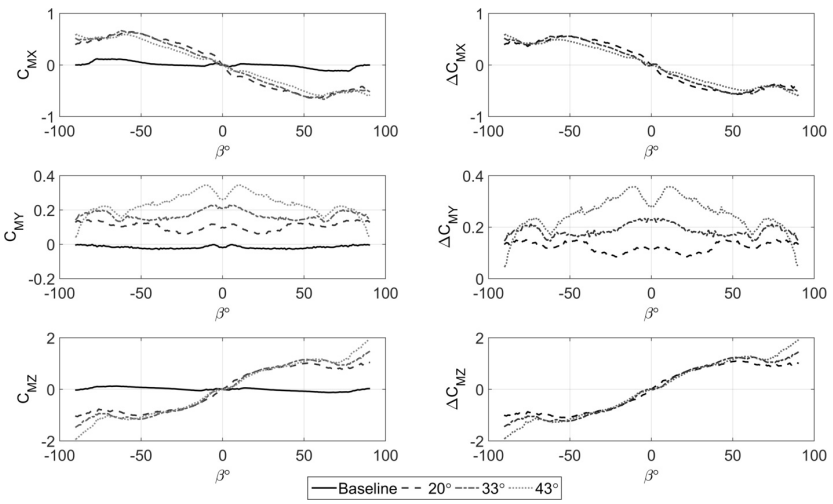
3.2 Stabilised CONEX wind-tunnel test results

Figures 12(a), 12(b), 13(a) and 13(b) present the stabilised load aerodynamic coefficients as functions of the sideslip angle for the various fin inclination angles tested. Data are presented for angles-of-attack of –10° and –35° that correspond to flight speeds of 40kt and 110kt respectively, as measured during flight tests with a 2,000lb CONEX cargo container fitted with 33° fins. The figures on the left column present the data for the fin stabilised load with the three fin inclination angles tested. The net load's aerodynamic coefficients are also included for reference ('baseline' – load without fins). The figures on the right column show the incremental aerodynamic effect of fins addition to the net load, and were calculated by subtracting the net load's aerodynamics from that of the total load's, as implied by Equation (9). The load model's width and frontal area of 16·8cm and 295·7cm^2 respectively, were used as the reference length and area for aerodynamic coefficients calculations. The custom convention of presenting aerodynamic properties in wind axes was abandoned here in favor of presentation in load fixed axes. It is assumed that the origin of these axes is located in the net load's geometric centre, with the x-axis pointing forward, y-axis pointing right, and z-axis pointing down. This 'switch' in the reference co-ordinate system was done since it is felt that for aerodynamic problems that involve a wide range of angles-of-attack and sideslip, analysis becomes much more natural and convenient using this system, than in the case of using the wind co-ordinate system. This observation (that was also made by Greenwell[7] as mentioned earlier), stems mainly from the flow pattern around bluff bodies, in which the normal pressure loads on the cubic faces are much larger than the tangential loads, turning the traditional use of wind co-ordinate system somewhat artificial. Comparison of Figs 12 and 13 shows that the fins effect on the total aerodynamic force coefficients of the stabilised load is similar for different angles-of-attack. As expected, the axial force coefficient increases with increasing fin inclination angle due to the obvious increase of fins drag as this angle grows. The normal force coefficient also increases with increasing fin inclination angle, although this change is less apparent.

https://doi.org/10.1017/S0001924000011143 Published online by Cambridge University Press



(a) Aerodynamic force coefficients.



(b) Aerodynamic moment coefficients.

Figure 13. Stabilised load aerodynamic coefficients for three fin angles (20°, 33° & 43°), angle-of-attack = –35°.

Two interesting effects can be observed in the normal force coefficient (C_z) curves of Figs 12(a) and 13(a). The first is the decrease in this coefficient for sideslip angles higher than 35°, that can be attributed to the box length and width switching roles. This results in an increase in the portion of the separated flow region above the box, creating a decrease in the local static pressure. The second effect is the change in the normal force coefficient with sideslip angle near the origin, for low angles-of-attack. This is probably due to reattachment of the flow on the windward face, which in turn increases the average pressure on the upper face.

The most important incremental force component generated by the fins is the side force, since it is the one responsible for the generation of a restoring (stabilising) aerodynamic yaw moment with respect to the load's centre, once a sideslip angle different than zero is evolving. Unfortunately, in addition to this favorable stabilising effect, the development of side force also induces lateral pendulum motions of the load. This explains the reason for the combined lateral-directional

https://doi.org/10.1017/S0001924000011143 Published online by Cambridge University Press

character of stabilised load dynamics, once disturbed from equilibrium. A very interesting conclusion drawn from examination of the side force curves is somewhat surprising: it appears that the incremental side force created due to fins installation in the sideslip angle range of –40° to 40°, is almost insensitive to fin inclination angle (for the inclination angles tested). This feature of the data was observed in all the tested range of angles-of-attack. An accurate explanation of the reason for this behaviour requires extensive research through either CFD analysis or the use of flow visualisation techniques. Still, an intuitive understanding can be gained, by noticing that the fins mounted on the rear corners of the CONEX cargo container are not operating as isolated lifting surfaces but rather as 'flaps', being an extension of the side faces of the load. Calculation of the 'effective'section inclination angle resulting by joining the CONEX forward corner with the adjacent fin trailing edge produces 'section' angles of 4·2°, 5·6° and 6·3° for the fin inclination angles of 20°, 33° and 43°, respectively. The maximum 'camber' of the resulting section 'aerofoils' are 0·054, 0·071 and 0·081. Hence, all three fin inclination angles produce a very similar 'aerofoil' cross section, which in turn leads to the flow being almost insensitive to fin inclination angle in the low-medium sideslip angle range. This explanation, although oversimplified, might give a clue as to how this effect is created.

Examination of the moment coefficients in Figs 12(b) and 13(b) leads to similar observations as those made for the force coefficients. A non-negligible roll moment coefficient (that is close to zero for the net CONEX) is developed due to the fins side force that is acting above the load's geometric centre. This in turn creates a negative roll moment slope. Similarly, the pitch moment curves are a reflection of the drag increase involved with increasing the fin inclination angles. Again, due to the fins centre of pressure location above the load centre, the fins drag force creates a positive pitch moment.

The fins stabilising effect is clearly seen in the yaw moment coefficient curves. Comparisons of the net load curve and the stabilised load curves show that the nearly neutrally directionally stable CONEX turns completely statically directionally stable when fins are mounted. As observed for the side force, it appears that the fins incremental yaw moment is only slightly dependent on fin inclination angle at low-medium sideslip angles. This rather surprising result seems to contradict dynamic wind-tunnel test results that clearly demonstrated better stability as fin inclination angle increased. The following text provides an explanation attempting to clarify the supposed contradiction.

Dynamic wind-tunnel tests showed[1, 24, 31] the existence of yaw-roll limit cycle oscillations (LCO). These will be elaborated with significant detail in a follow-on paper. Yet, the characteristics of this dynamic mode can be understood from a close examination of the yaw moment coefficient curves. Figure 14 presents a close-up of the total and incremental yaw moment coefficient for angles-of-attack of –10° and –35°. For a low angle-of-attack of –10° it can be seen that the fins have a destabilising effect. As a result, the total stabilised load yaw moment slope is very shallow for the 43° fins, and negative for the 20° and 33° fins. This negative slope (for the last two fin angles) leads to the load having three equilibrium (trim) points: an unstable equilibrium at a sideslip angle of 0°, and two stable equilibria at sideslip angles of ≈ ±2°. The characteristic dynamics of this system is such that once the load is disturbed from equilibrium, LCO will develop, which will be manifested by coupled yaw-roll oscillations (this is demonstrated later in Section 4.0). When the angle-of-attack is increased from –10° to -35°, the CONEX configuration with 20° fins turns stable as well, and the 33° fin configuration is still locally unstable at the origin. Due to the higher fin drag associated with larger fin inclination angles, the CONEX trim angle-of-attack (load trail angle) grows in absolute value with increasing fin inclination angles, therefore exposing a larger part of the fins to the undisturbed free stream, and increasing fins efficiency as a result. Thus,

https://doi.org/10.1017/S0001924000011143 Published online by Cambridge University Press

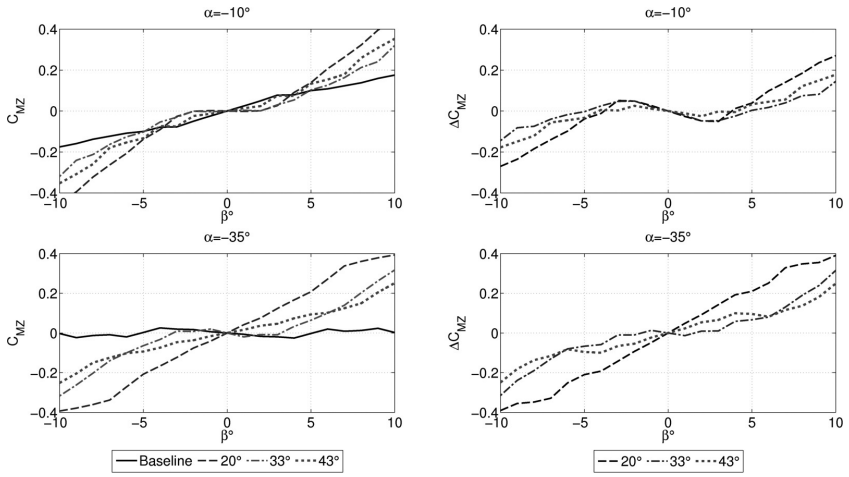


Figure 14. Close-up of stabilised CONEX yaw moment coefficient.

for the same airspeed, larger fin inclination angles are more efficient for load stabilisation. This explains how the increase of fin inclination angle enhances stabilisation.

3.3 Aerodynamic model formulation – initial approach

In order to produce an aerodynamic model for a stabilised CONEX with any desired fin inclination angle, it was originally planned to use the incremental fin aerodynamic database for the extraction of the aerodynamic interference between the load's aft section and the fins. Proper correction terms would then be applied to the isolated fin database, to provide the rear mounted fins aerodynamic coefficients (as will be demonstrated later in Section 4.0, when no such corrections are applied, the fins efficiency as stabilising devices is over predicted). If successful, this process would have created a generic capability for the prediction of the aerodynamic characteristics of box-shaped loads that are stabilised by rear mounted fins. It was perceived that during simulation, the stabilised slung load's aerodynamic coefficients would be accumulated by separately predicting the net load, right fin and left fin aerodynamic loads (with proper corrections to account for load/fins interference effects), assuming quasi-steady aerodynamics (i.e. correcting the flow airspeed components to include the effect of load angular rates). Numerous different models for accounting for the combined load plus fins aerodynamics were attempted, which description is beyond the scope of the current paper. Some of the methodologies studied (separately, or in conjunction with each other) were:

1. Introduction of dynamic pressure 'efficiency' factors for the right and left fins.
2. Calculation of the stabilised load centre of pressure location for use as a reference point for airspeed components calculation.
3. Calculation of the combined fins centre of pressure location for use as a reference point for the combined fins aerodynamic contribution.
4. Transport time delays for load and/or fins airspeed components.
5. Introduction of a geometrically based fin blocking effect, due to the load, as a function of load angles-of-attack and sideslip.
6. Calculation of correction terms for the right and left fins vertical force coefficients (ΔC_{z_1}, ΔC_{z_2}), and for the net load's side force coefficient ΔC_y.

https://doi.org/10.1017/S0001924000011143 Published online by Cambridge University Press

The efficiency of these models was assessed using comparisons between model predictions and the static aerodynamic wind-tunnel data available for the stabilised CONEX, as well as comparisons between dynamic simulations and dynamic wind-tunnel test results. As explained above, the predicted resultant stabilised load aerodynamic database was assembled by first adding up the aerodynamic contributions of its components (net load, right fin and left fin). Then, load/fins interference effects were added to the resulting model as aerodynamic corrections, to complete the assembly of the stabilised load aerodynamic database. Most of the simulation results obtained by using the methodologies described above, did not show satisfactory agreement with dynamic wind-tunnel test results. An exception to this is the sixth methodology listed (correction of fins $\Delta C_{z_{1/2}}$ and net load ΔC_y), which gave good prediction for the pitch and roll angles time histories, but under predicted the oscillations periods and the yaw angle amplitudes[29]. This methodology can be therefore used for preliminary predictions of fin stabilised load dynamics, in cases where no other data are available for the stabilised load aerodynamics. Based on similarity considerations, the force coefficients correction terms can be added to the net load and isolated fins aerodynamic databases, respectively. Then, the aerodynamic coefficients of these components can be added together to provide an initial estimation of the stabilised load's aerodynamic database.

Following analysis of the resulting force coefficients correction terms described above ($\Delta C_{z_{1/2}}$ and ΔC_y), it was concluded that as could be initially expected, the main aerodynamic interference between the net load and the fins is developed on the load side faces, and influences the pressure distribution on these faces and adjacent fins. As a result, the side forces produced by each of these aerodynamic surfaces change. In addition, it is also reasonable to expect that the net load centre of pressure moves further aft from its assumed geometric position, thus introducing a change in the net load yaw moment as well. These results lead to the conclusion that viewing the stabilised CONEX as an 'aerodynamic multi body' whose aerodynamic characteristics are of additive nature, is over simplistic. Therefore, a different approach should be attempted.

3.4 Aerodynamic model formulation – revised approach

As presented above, the initial approach of accumulating the 'isolated' aerodynamics components of the stabilised load provided unsatisfactory results. This is attributed to the mutual aerodynamic interference between the load and the fins being much more complex than initially expected. Therefore it is suggested that the fins stabilised load should be viewed as a completely new load, rather than as a 'modification' of the net load. Using the stabilised load static aerodynamic database as measured directly in the wind-tunnel might be a more correct approach, as compared to trying to assemble it from its aerodynamic components.

Dynamic simulation was used as the main tool for assessment of this approach. As a first step, simulation using the stabilised load static aerodynamic database was attempted (the results will be shown in the following section). Comparison of these results to reference dynamic wind-tunnel tests showed that fins effectiveness is under evaluated. Specifically, it appeared that the fins damping effect is under predicted.

Due to the inadequacy of predicting the stabilised load's dynamics using the wind-tunnel measured static aerodynamic coefficients, it was suggested next to treat the fins damping effect separately. In order to achieve this it was assumed that the incremental aerodynamic loads due to the load's rotation about its centre of gravity (cg) are mainly attributed to the fins, with the aerodynamic damping of the CONEX itself being much lower. The total stabilised load aerodynamic coefficients were thus calculated by the following steps:

Step 1: The stabilised load static aerodynamic coefficients ($(\bar{C}_{AER})_{LOAD+FINS,STATIC}$) were interpolated from the wind-tunnel static database. The net load's geometric centre was used as the reference

https://doi.org/10.1017/S0001924000011143 Published online by Cambridge University Press

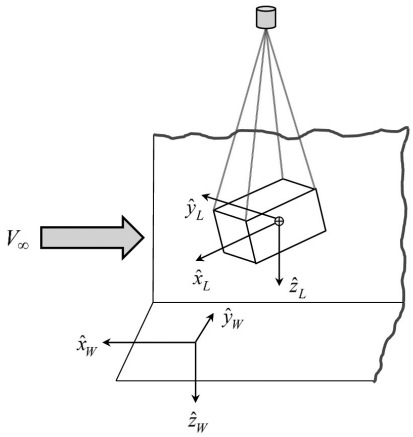


Figure 15. Wind and load co-ordinate systems.

point for determination of the inertial velocity components (which affect angle-of-attack, sideslip angle and dynamic pressure).

Step 2: The net fins contribution to the stabilised load aerodynamic coefficients ($(\Delta\bar{C}_{AER})_{FINS}$) was calculated using the fins aerodynamic centres as the reference points for determination of the aerodynamic properties (each fin was evaluated separately).

Step 3: The previous step was repeated assuming zero angular rates, to obtain $(\Delta\bar{C}_{AER}))_{FINS,STATIC}$.

Step 4: The fins 'dynamic increment' due to angular rates was calculated by using the following equation:

$$(\Delta\bar{C}_{AER})_{FINS,DYNAMIC} = (\Delta\bar{C}_{AER})_{FINS} - (\Delta\bar{C}_{AER})_{FINS,STATIC} \quad \ldots (10)$$

Here, it was assumed that the fins incremental aerodynamics is comprised of a 'static' part where no angular rates are present, and a 'dynamic' part that includes the loads associated with angular rates.

Step 5: The fins dynamic increment was added to the stabilised load aerodynamic coefficients (calculated in the first step) to provide the total stabilised load aerodynamic coefficients:

$$(\bar{C}_{AER})_{LOAD+FINS,TOTAL} = (\bar{C}_{AER})_{LOAD+FINS,STATIC} + (\Delta\bar{C}_{AER})_{FINS,DYNAMIC} \quad \ldots (11)$$

4.0 DYNAMIC SIMULATION

4.1 Simulation description

In order to allow the validation of the fins stabilised CONEX aerodynamic model, a dynamic simulation representing a slung load in wind-tunnel (see Fig. 3) was programmed in MATLAB. The load equations of motion were formulated in the load fixed co-ordinate system (L) centred at the load's cg, with the x-axis pointing forward, y-axis pointing right, and z-axis pointing down. An inertialy fixed wind-tunnel co-ordinate system (W) was also used, with the x-axis aligned with the tunnel longitudinal axis and pointing into the incoming flow, y-axis pointing right (normal to the tunnel side walls) and z-axis pointing down. Refer to Fig. 15 for co-ordinate systems definition.

https://doi.org/10.1017/S0001924000011143 Published online by Cambridge University Press

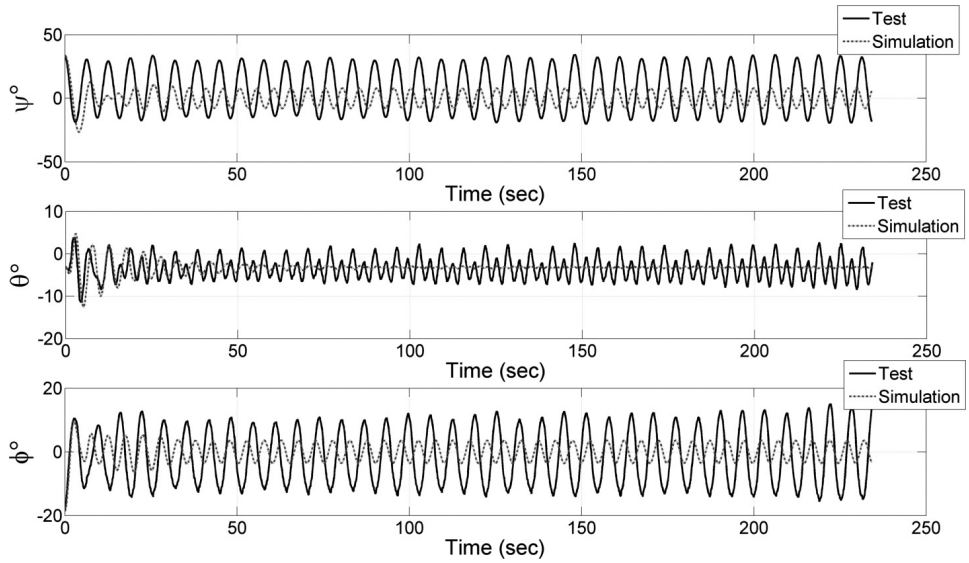


Figure 16. Comparison between test results and simulation predictions, no correction for load/fin interference, 6ms^{-1}.

The transformation from wind axes to load axes follows the conventional flight dynamics rotation order of Euler angles: Yaw (ψ) → Pitch (θ) → Roll (ϕ). For the test data these angles were calculated from the gimbal angles time histories recorded during the dynamic wind-tunnel tests[24,25], which follow a different rotation sequence. Swivel friction was assumed negligible, as was validated by checking the load's yaw rate decay, following application of initial spin rate to the load during wind off conditions. The load's six degrees of freedom equations of motion are presented in Appendix B.

In the next subsection, simulation output results are presented for a full scale 2,000lb CONEX cargo container fitted with 33° fins. The effective pendulum length (the vertical distance between the wind-tunnel's ceiling to the model's cg) was 1·85ft (0·56 m), and corresponds to a full scale length of 20·3ft (6·19m). In order to allow the comparison between simulation predictions and wind-tunnel test results, the test data of the 1:11 scale model, should be scaled up using Froude scaling: Wind-tunnel speed and test running time are multiplied by $\sqrt{11}$ (see Raz *et al*[24] for details). In the figures that follow, full scale time is used. As the main indication of slung load stability is perceived as its tendency to return to equilibrium once disturbed, the correspondence between test results and simulation predictions was judged by comparing the qualitative nature of disturbed load dynamics, and associated oscillation amplitudes, frequencies and damping ratios.

4.2 Simulation results

The original objective of the effort described in this paper was to enable the prediction of the fins stabilised load aerodynamic characteristics by combining separate 'isolated' aerodynamic models for the load and right and left fins, and correcting each of them for interference effects. If successful, this would have allowed the prediction of quasi-steady aerodynamic damping due to fins addition, by considering each fin's local velocity components that are strongly dependent on the load's angular rates.

https://doi.org/10.1017/S0001924000011143 Published online by Cambridge University Press

In order to demonstrate the significance of the load/fins interference effects, the simulation was first run by adding the net load and isolated fins aerodynamic coefficients, to create an aerodynamic database representing the fins stabilised load. The assembly of this database was done assuming no interference exists between the load's rear section and the fins. Fig. 16 presents a comparison between simulation results and dynamic wind-tunnel test results for this 'no interference' case study. The average wind-tunnel speed for this run is approximately 6ms^{-1}, which corresponds to a full scale airspeed of 38·5kt. The CONEX model is initially held fixed at offset yaw, pitch and roll angles with respect to the wind-tunnel axes, and then released. It can be observed that for this low airspeed, limit cycle oscillations (LCO) are evident in the test results for all three axes. Yaw angle amplitudes are close to 25°, and roll angle amplitudes are ~13°. Due to the cross axes coupling caused by load drag increase with increasing sideslip angle, LCO are also present in the pitch angle, although with lower intensity and twice the yaw/roll oscillations frequency. The simulation correctly predicts the creation of stable LCO in these conditions. However, the predicted amplitudes are much lower than those recorded during the test. The predicted pitch motion is close to a damped response of a second order system, and only a close examination of the time history plots shows the presence of very weak LCO in this axis as well. A significant difference exists between predicted and recorded LCO frequencies. This is demonstrated by the predicted yaw LCO frequency of 0·2Hz as compared to a recorded frequency of 0·16Hz. These frequencies are average, since the actual dynamics of the load is highly nonlinear.

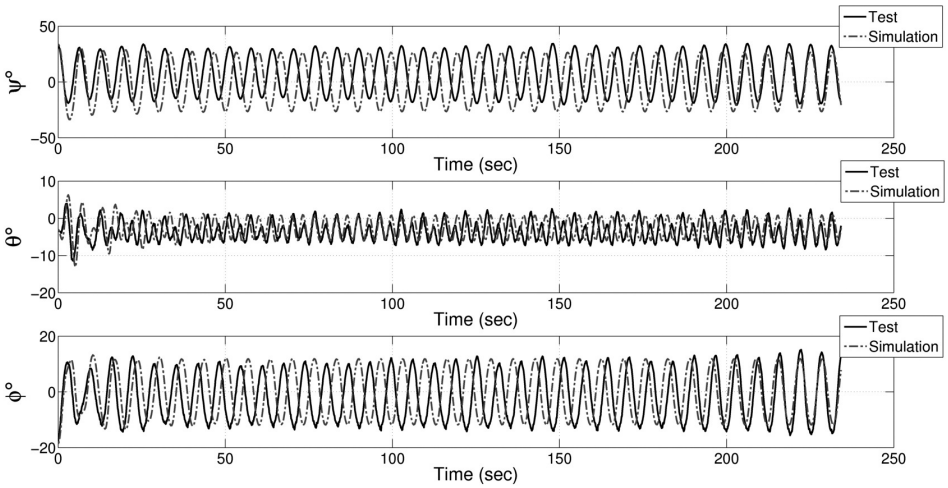
This basic comparison demonstrates the importance of incorporating an aerodynamic correction to the fin database, to account for load/fin interference effects. The under prediction of LCO amplitudes and over predictions of pitch damping and yaw/roll frequency, suggests that actual fin efficiency should be lower than that calculated assuming no interference. Similar conclusions were drawn after similar comparisons at higher airspeeds, where the load is stable. The simulation predicted stronger damping and faster decay to steady state equilibrium than those observed during wind-tunnel tests.

As described earlier, following the unsatisfactory results received using the 'aerodynamic multi body' approach, it was decided to try and use the complete stabilised load's static aerodynamic coefficients. An aerodynamic database for the stabilised CONEX was obtained using the measurements from static wind-tunnel tests, without any additional corrections or adjustments. The load's incoming flow components were corrected to account for the incremental local flow components induced by the load's cg oscillations. This introduced quasi-steady effects into the model, as it affected the dynamic pressure and the aerodynamic angles during the simulation.

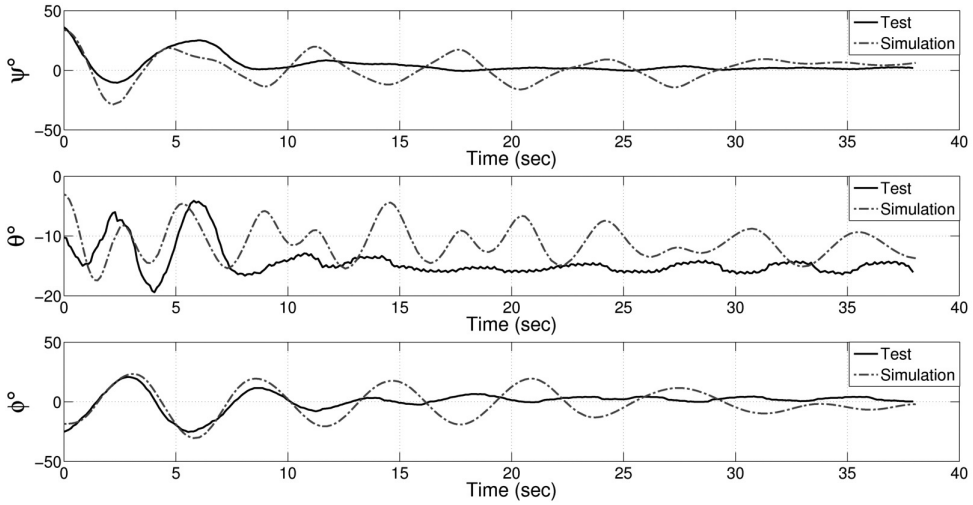
Figure 17(a) repeats the comparison that was presented in Fig. 16, for the case of using the measured stabilised load aerodynamic database, instead of accumulating it from its components. Although the predicted LCO amplitudes in Fig. 17(a) are now close to test results (predicted yaw and roll amplitudes of 27·8° and 12·6° respectively, as compared to the corresponding test results of 25° and 13°), the calculated frequency of the oscillations is lower than measured (0·15Hz predicted, versus 0·16Hz measured). Figure 17(b) shows the same comparison for a higher wind-tunnel speed of 9ms^{-1}, which corresponds to 58kt full scale airspeed. At this speed the LCO disappear and the disturbances subside. It can be observed that the fins effectiveness is under predicted. While actual test results show strong damping of the load motion (damping ratio of 10·6%), simulation results are much more oscillatory in nature (damping ratio of 3·1%). The damping ratios were calculated using the roll angle time history.

The reason for these results can be explained by the fact that all the aerodynamic properties of the stabilised load (i.e. angle-of-attack, sideslip angle and dynamic pressure) are calculated at the net load's geometric centre, which served as the reference point for aerodynamic loads measurement.

https://doi.org/10.1017/S0001924000011143 Published online by Cambridge University Press



(a) 6ms^{-1}



(b) 9ms^{-1}

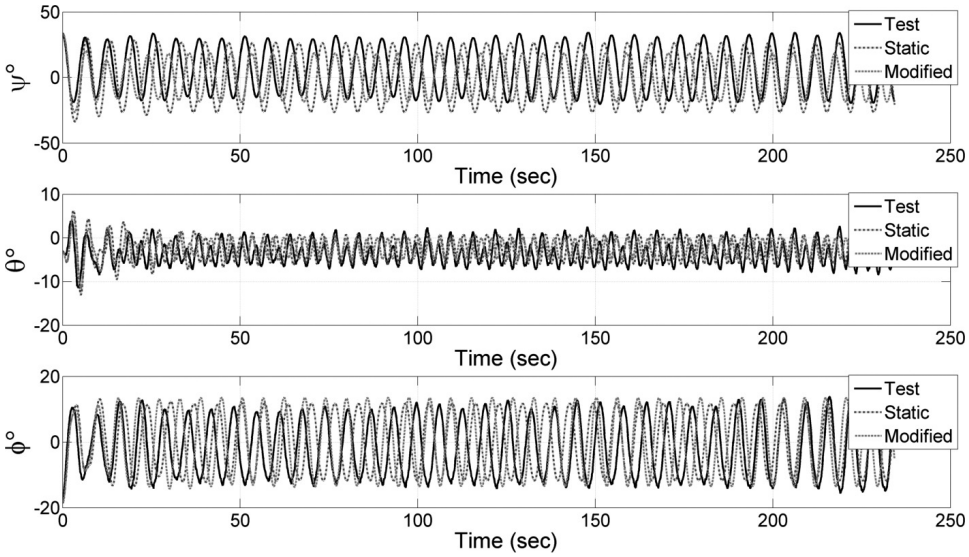
Figure 17. Comparison between test results and simulation predictions using static wind tunnel data for stabilised CONEX aerodynamic model.

This point is way forward of the fins actual ac. Therefore, the fins damping effect, which is highly dependent on the fins ac's arms with respect to the load cg, is only partly accounted for.

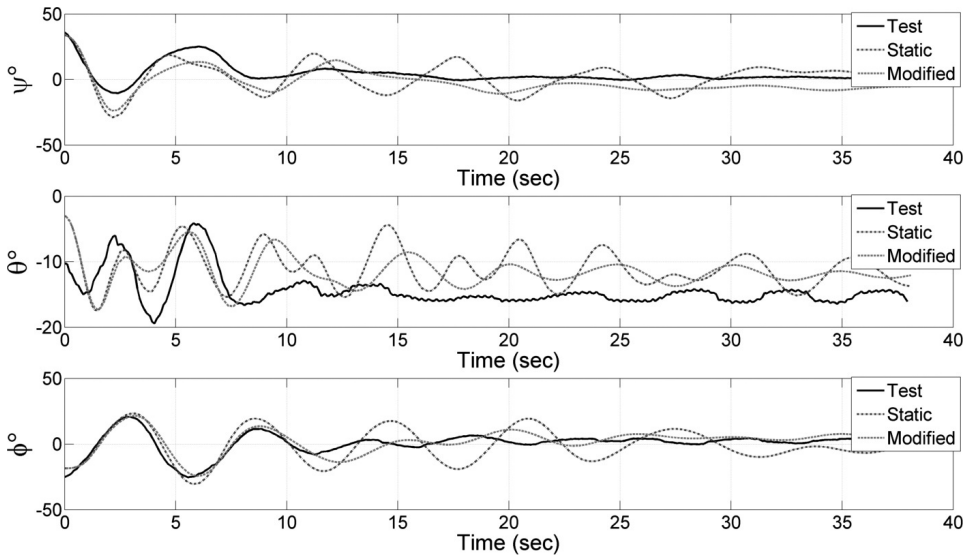
In order to supplement the fins contribution to the load's damping, it was next attempted to treat the fins damping effect separately. As described in Section 3.4, a fins 'dynamic increment' was calculated, and added to the net load's aerodynamic forces and moments.

Figures 18(a,b) include the results that were presented in Fig. 17(a,b), with the addition of the dynamic increment correction. The former simulation results are designated 'Static' and the new

https://doi.org/10.1017/S0001924000011143 Published online by Cambridge University Press



(a) 6ms^{-1}

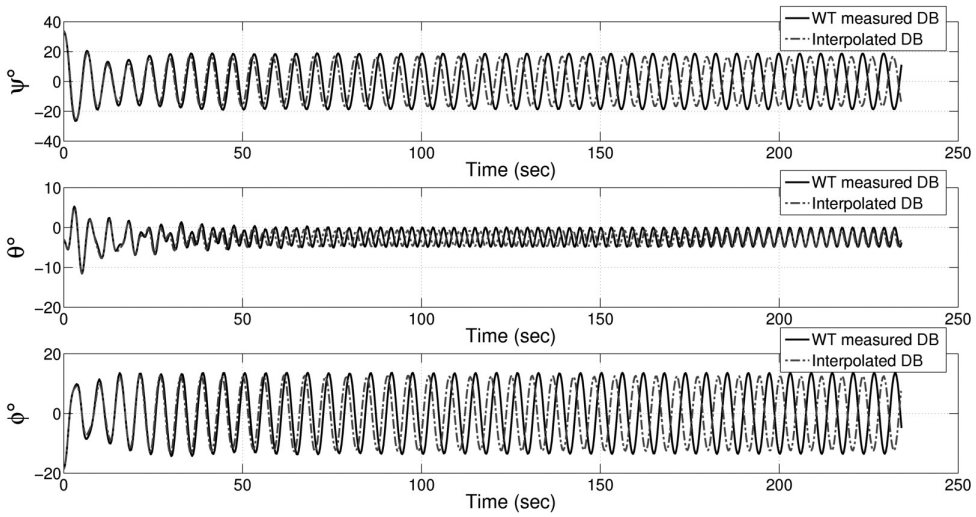


(b) 9ms^{-1}

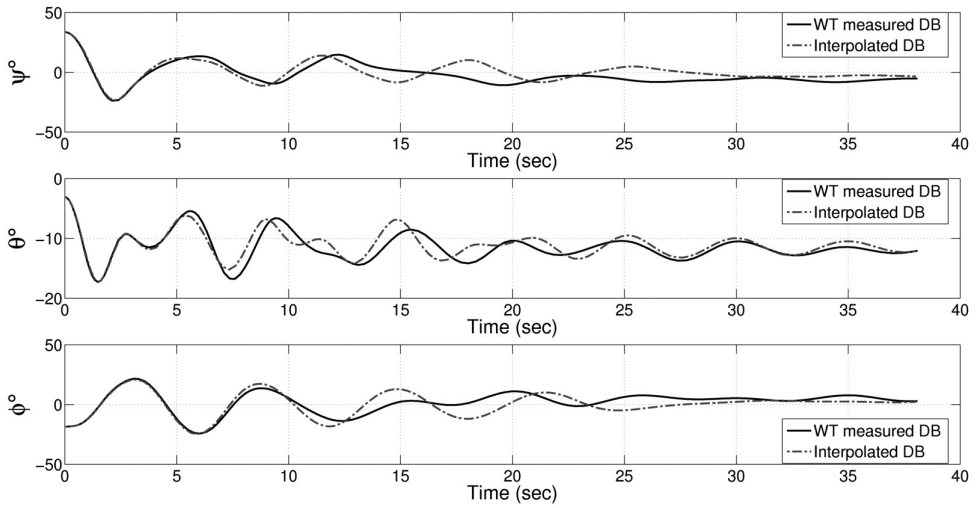
Figure 18. Comparison between test results and simulation predictions using static wind tunnel data for stabilised CONEX aerodynamic model.

results are designated 'Modified'. From Fig. 18(a) it is concluded that both models are successful in predicting the LCO in all three axes. The modified model under predicts the yaw amplitude and over predicts the oscillation frequency (19·1°/0·17Hz predicted, versus 25°/0·16Hz from test results). The opposite is true for the static model. Thus, it is not possible to favor one model over the other

https://doi.org/10.1017/S0001924000011143 Published online by Cambridge University Press



(a) 6ms^{-1}



(b) 9ms^{-1}

Figure 19. Comparison of simulation results for wind-tunnel measured and interpolated databases, fin inclination angle 33°.

based on the results for 6ms^{-1}. Contrary to this, the results for a wind-tunnel speed of 9ms^{-1} that are presented in Fig. 18(b) demonstrate that the modified model provides better agreement with test data in term of the aerodynamic damping prediction. With the modified model, the predicted damping ratio (based on roll angle time history) is increased to 7·5%, which is closer to the test measured value of 10·6% than the value predicted earlier using the static model. These conclusions were confirmed using available data for other fin inclination angles (20° and 43°) and load

https://doi.org/10.1017/S0001924000011143 Published online by Cambridge University Press

weight (4,000lb). It is noted that the frequencies of the LCO (Fig. 18(a), 0·17Hz) and the damped oscillation (Fig. 18(b), 0·16Hz) are very close. This indicates that these frequencies are mainly driven by the basic lateral pendulum frequency. The small impact of airspeed on the resulting oscillation frequencies were observed in previous tests[25].

It is thus concluded that by using the wind-tunnel static aerodynamic database for the complete configuration (load and fins) and applying a 'dynamic increment' correction to this database, it is possible to obtain an aerodynamic representation suitable for use in dynamic simulations. It should be emphasised that no interference correction is applied to the fins dynamic increment correction, so that the fins aerodynamic contribution is calculated using the tuned isolated fin database described in Section 2. Therefore, if a stabilised load's aerodynamic coefficients are mapped in a wind-tunnel test for a small set of pre-determined fin inclination angles, an aerodynamic database for any desired fin inclination angle in the tested domain can be computed using simple interpolation.

4.3 Validation of aerodynamic database interpolation

In order to demonstrate the database prediction method for an interim fin inclination angle, the measured stabilised CONEX databases for 20° and 43° fin inclination angles were linearly interpolated to provide an estimated database representative of a stabilised CONEX with a fin inclination angle of 33°. Simulation using the interpolated database was repeated, with results compared to those predicted using the accurate database for the same fin inclination angle, that was derived from direct wind-tunnel test measurements.

The results presented in Figs. 19(a) and 19(b) for wind-tunnel speeds of $6ms^{-1}$ and $9ms^{-1}$ respectively, demonstrate the validity of using interpolated aerodynamic databases. For the $6ms^{-1}$results, predictions using the interpolated database result in the yaw LCO average frequency being 1·5% higher than that predicted by the accurate database. The resulting yaw amplitude for this wind speed is 16·6°, which is 11% lower than the accurate database prediction of 18·6°. Similar results are seen in the pitch and roll axes as well. Comparison of results for a wind speed of $9ms^{-1}$ show that interpolated load damping (5·1%) is predicted lower than when using of the accurate database (7·5%). Still, the overall characteristics of load dynamics following its release from the initial position is very similar, with peak yaw, pitch and roll angles as well as equilibrium position angles being very close. Hence, it is concluded that the proposed method could be applied for fins stabilised load configuration, requiring only a limited set of wind-tunnel tests of the fins stabilised load for different fin inclination angles. This data can then be used for aerodynamic predictions for any required fin inclination angle within the tested range.

5.0 CONCLUSIONS

- Satisfactory prediction of the aerodynamic loads of an isolated flat plate fin is achieved for a wide range of angles-of-attack and sideslip, by tuning the plate's average upper surface pressure coefficient using wind-tunnel measurements. The aerodynamic pitch and roll moments are under predicted, but are of secondary importance for the prediction of incremental aerodynamic loads due to fins installation on a slung load.
- Analysis of bluff body aerodynamics in body fixed axes is preferred to analysis in wind axes, due to the large range of angles-of-attack and sideslip angles in which normal pressure loads rather than lift forces are acting on the subject load's faces.

https://doi.org/10.1017/S0001924000011143 Published online by Cambridge University Press

- The stabilising yaw moment contributed by rear mounted fins is nearly independent of fin inclination angle for low and medium sideslip angle, at a given angle-of-attack. However, due to the higher drag induced by larger fin inclination angles, equilibrium angle-of-attack increases (in absolute value) with increasing fin inclination angle, thus exposing larger parts of the fins to the undisturbed flow. Hence, larger fin inclination angles are more efficient for load stabilisation purposes but induce a larger drag penalty.
- The method of combining static wind-tunnel measurements for a stabilised load, with a theoretical correction term for the fins 'dynamic' contribution, can be used for predicting stabilised loads dynamic behaviour. Simulation of a slung load using this method provides results that are both qualitatively and quantitatively close to dynamic wind-tunnel test results.
- The described method can be applied in cases where optimal fin inclination angle for a given load is to be determined. The combination of a relatively small set of static wind-tunnel tests, together with a theoretical correction of the fins aerodynamic contribution due to load angular rates, enables creation of approximated aerodynamic databases for interim fin inclination angles not tested in the tunnel.
- The present paper uses dynamic simulation as a tool for estimating the suitability of the proposed aerodynamic load databases for prediction of stabilised slung load dynamics. This highly nonlinear dynamic system possesses complex characteristics such as LCO, multi equilibrium points, quasi periodicity of solutions and more. These issues are out of scope of the present paper and are planned to be covered in separate dedicated publications.

ACKNOWLEDGEMENT

The Authors would like to thank Mr A. Beer and the wind-tunnel team of the Faculty of Aerospace Engineering at the Technion, for their support during the wind-tunnel tests.

REFERENCES

1. CICOLANI, L.S., RAZ, R., ROSEN, A., GORDON, R., CONE, A., THERON, J. N., LUSARDI, J., TIRCHLER, M. and ROBINSON, D. Flight test, simulation and passive stabilization of a cargo container slung load in forward flight, American Helicopter Society International 63rd Annual Forum, 1-3 May 2007, **3**, pp 2177-2206, Virginia Beach, VA, USA.
2. SHELDON, D.F. Appreciation of dynamic problems associated with external transportation of loads from a helicopter-state of art, *Vertica*, 1977, **1**, (4), pp 281-290.
3. PRYOR, J. and SHELDON, D.F. Phase 2 – a study in depth of a single point and two point lateral and tandem suspension of rectangular box loads, May 1973, RMCS Technical Note AM 38, Royal Military College of Science.
4. SIMPSON, A. and FLOWER, J.W. Unsteady aerodynamics of oscillating containers and application to the problem of dynamic stability of helicopter underslung loads, May 1978, AGARD CP 235.
5. WATKINS, T.C., SINACORI, J.B. AND KESLER, D.F. Stabilization of externally slung helicopter loads [Final Report, 1 Jul 1972-31 Oct 1973], Final Report, August 1974, USAAMRDL-TR-74-42, US Army MRDL.
6. SAMPATH, P. Dynamics of a Helicopter-Slung Load System, PhD thesis, April 1980, University of Maryland, USA.
7. GREENWELL, D.I. Modelling of static aerodynamics of helicopter underslung loads, 2008, 26th Congress of International Council of the Aeronautical Sciences, 14-19 September 2008, , ICAS 2008-5.11.2, Anchorage, AK, USA.
8. THERON, J.N., DUQUE, E.P.N. and CICOLANI, L. A CFD Study of the aerodynamics of a 6 × 6 × 8 foot cargo container suspended beneath a helicopter, Part I: Aerodynamics of the stationary container, October 2007, AFDD/TR-07-001, US Army AFDD.

https://doi.org/10.1017/S0001924000011143 Published online by Cambridge University Press

9. CICOLANI, L.S., CONE, A., THERON, J.N., ROBINSON, D., LUSAARDI, J., TISCHLER, M.B., ROSEN, A. and RAZ, R. Flight test and simulation of a cargo container slung load in forward flight, *J American Helicopter Soc*, 2009, **54**, (3), pp 0320061-03200618.
10. MNATRI, R., RAGNAV, V., KOUKOL, B., KOMERATH, N. and SMITH, M. Study of factors driving pitch, roll, and yaw coupling in bluff body aerodynamics, 2011, 41st AIAA Fluid Dynamics Conference and Exhibition, 27-30 June 2011, Honolulu, Hawaii, USA.
11. PROSSER, D.T. and SMITH, M.J. Characterization of flow around rectangular bluff bodies at angle of attack, *Physics Letters A*, August 2012, **376**, (45), pp 3204-7.
12. LIU, D.T. In-flight stabilization of externally slung helicopter loads, Final Report, June 1970-June 1972, USAAMRDL Tech. Report 73-5, May 1973, US Army Air Mobility Research and Development Labs, Fort Eustis Directorate, Fort Eustis, VA, USA.
13. ASSEO, S.J. and WHITBACK, R.F. Control requirements for sling-load stabilization in heavy lift helicopters, *J American Helicopter Soc*, July 1973, **18**, (3), pp 23-31.
14. MICALE, E.C. and POLI, C. Dynamics of slung bodies utilizing a rotating wheel for stability, *J Aircr*, 1973, **10**, (12), pp 760-763.
15. FEASTER, L.L. Dynamics of a Slung Load, PhD thesis, June 1975, Massachusetts University, Amherst, MA, USA.
16. PARDUE, M.D. and SHAUGHNESSY, J.D. Design and analysis of an active jet control system for helicopter sling loads, January 1979, NASA TP 1397.
17. NAGABHUSHAN, B.L. Optimal controller design for a helicopter using its lower order dynamic model, American Institute of Aeronautics and Astronautics, Aircraft Design, Systems and Technology Meeting, 17-19 October 1983, Fort Worth, TX, USA.
18. RAZ, R., ROSEN, A. and RONEN, N.T. Active aerodynamic stabilization of a helicopter sling-load system, *J Aircr*, September 1989, **26**, (9), pp 822-828.
19. EHLERS, G.E. Hi-fidelity Simulation and Prediction of Helicopter Single Point External Load Stabilization, MSc thesis, September 2001, Naval Postgraduate School, Monterey, CA, USA.
20. HAMERS, M. and BOUWER, G. Flight director for helicopter with slung load, 30th European Rotorcraft Forum, 14-16 September 2004, pp 795-804, Marseilles, France.
21. HAMERS, M. and BOUWER, G. Helicopter slung load stabilization using a flight director, American Helicopter Society International 60th Annual Forum, 1-3 June 2005, **1**, pp 768-780, Grapevine, TX, USA.
22. HAMERS, M. Flight director for handling of helicopter sling loads, 2005, 31st European Rotorcraft Forum, 13-15 September 2005, pp 119.1-119.11, Florence, Italy.
23. HAMERS, M., VON HINUBER, E. and RICHTER, A. Flight director for slung load handling – First experiences on Ch53, 33rd European Rotorcraft Forum, 11-13 September 2007, **4**, pp 2557-2566, Kazan, Russia.
24. RAZ, R., ROSEN, A., CARMELI, A., LUSARDI, J., CICOLANI, L.S. and ROBINSON, L.T.C.D. Wind tunnel and flight evaluation of stability and passive stabilization of cargo container slung load, American Helicopter Society International 64th Annual Forum, 29 April-1 May 2008, **2**, pp 1097-1126, Montreal, Canada.
25. RAZ, R., ROSEN, A., CICOLANI, L.S., LUSARDI, J., GASSAWAY, B. and THOMPSON, T. Using wind tunnel tests for slung loads clearance, 67th American Helicopter Society International Annual Forum, 3-5 May 2011, pp 3110-3137, Virginia Beach, VA, USA.
26. RINGLAND, R.F., TUSSCHLER, M.B., JEX, H.R., EMMEN, R.D. and ASHKENAS, I.L. Flight dynamics analysis and simulation of heavy lift airships. Volume 2: Technical Manual [Final Report, Sep 1979-Dec 1982], December 1982, NASA-CR-166471.
27. WICK, B.H. Study of the subsonic forces and moments on an inclined plate of infinite span, June 1954, NACA TN 3221.
28. HOERNER, S.F. *Fluid-Dynamic Drag*, 1965, Published by the Author, Bakersfield, CA, USA.
29. ENCIU, K. and ROSEN, A. Aerodynamic modeling of fin stabilized underslung loads, September 2013, TAE 989, Faculty of Aerospace Engineering, TECHNION – Israel Institute of Technology.
30. ROSEN, A., CECUTTA, S. and YAFFE, R. Wind tunnel tests of cube and Conex models, November 1999, TAE 844, Faculty of Aerospace Engineering, TECHNION – Israel Institute of Technology.
31. RAZ, R., ROSEN, A., CARMELI, A., LUSARDI, J., CICOLANI, L.S. and ROBINSON, D. Wind tunnel and flight evaluation of passive stabilization of a cargo container slung load, *J American Helicopter Soc*, July 2010, **55**, (3), pp 0320011-03200118.

https://doi.org/10.1017/S0001924000011143 Published online by Cambridge University Press

APPENDIX A: FIN AERODYNAMIC MODEL FORMULATION

The development of the fin's aerodynamic model uses similar principals to those used by Ringland *et al*[26], where the conventional use of the total dynamic pressure is abandoned in favor of using the dynamic pressure perpendicular to each relevant span. The model assumes that the moments and in plane forces (drag and side force) are dependent on modified dynamic pressures that do not include the corresponding lateral velocity component. Thus, the axial force and pitch moment are calculated using the expression $^1/_2\rho(u^2 + w^2)$ for the dynamic pressure, and the side force and roll moment are calculated using $^1/_2\rho(v^2 + w^2)$. The fin's aerodynamic forces and moments coefficients are first calculated by using the angle-of-attack α and drift angle γ, for determination of the appropriate flow region model to be used (i.e. linear, cross flow, or interpolation between the two). Using the modified expressions for the dynamic pressures, the fin's aerodynamic force and moment components are then calculated. Assuming the post stall region is defined by the angle-of-attack range $\alpha_{S1} < |\alpha| < \alpha_{S2}$, the force and moment coefficients for the x_F-z_F plane are:

Linear region $|\alpha| < \alpha_{S1}$:

$$\begin{aligned} &\text{(a)}\ C_L = C_{L\alpha}\alpha \\ &\text{(b)}\ C_D = C_{D0} + K \cdot C_L{}^2 \\ &\text{(c)}\ C_M = 0 \end{aligned} \qquad \ldots (A.1)$$

Cross flow region $|\alpha| > \alpha_{S2}$:

$$\text{(a)}\ x_{cp} = 0{\cdot}5 - (2 - 4x_{ac})\frac{\mathrm{Cos}|\alpha|}{4 + \pi\mathrm{Sin}\alpha} \qquad \ldots (A.2)$$

$$\text{(b)}\ C_{n_{xz}} = \frac{2\pi k\mathrm{Sin}|\alpha|}{4 + \pi\mathrm{Sin}|\alpha|} - Pu_{av}$$

$$\text{(c)}\ C_L = C_{n_{xz}}\mathrm{Cos}\alpha$$

$$\text{(d)}\ C_D = C_{n_{xz}}\mathrm{Sin}\alpha$$

$$\text{(e)}\ C_M = \frac{2\pi k\mathrm{Sin}|\alpha|}{4 + \pi\mathrm{Sin}|\alpha|}(x_{ac} - x_{cp}) + Pu_{av}(0{\cdot}5 - x_{ac})$$

$\alpha_{S1} \le |\alpha| \le \alpha_{S2}$— a trigonometric interpolation is used:

$$\text{(a)}\ C_{L/D/M} = \left(C_{L/D/M}(\alpha)\right)_{linear} \cdot p + \left(C_{L/D/M}(\alpha)\right)_{cross\ flow} \cdot (1 - p) \qquad \ldots (A.3)$$

where:

$$\text{(b)}\ p = 0{\cdot}5\left[1 + \mathrm{Cos}\left(\frac{|\alpha| - \alpha_{S1}}{\alpha_{S2} - \alpha_{S1}} \cdot \pi\right)\right]$$

The non-dimensional forces and moments are then calculated in fin axes to give:

$$\begin{aligned} &\text{(a)}\ C_x = -\frac{V_{xz}{}^2}{V_\infty{}^2}\left(-C_L\mathrm{Sin}|\alpha| + C_D\mathrm{Cos}|\alpha|\right)\cdot\mathrm{Sign}(u) \\ &\text{(b)}\ C_{z_{xz}} = -C_{n_{xz}} \cdot \mathrm{Sign}(w) \\ &\text{(c)}\ C_{M_y} = \frac{V_{xz}{}^2}{V_\infty{}^2}C_M \cdot \mathrm{Sign}(w) \end{aligned} \qquad \ldots (A.4)$$

https://doi.org/10.1017/S0001924000011143 Published online by Cambridge University Press

The reason for using the complete dynamic pressure for $C_{z_{xz}}$ calculation by Equation (A.4(b)) (unlike the practice for C_x and C_{MY} calculations by Equations (A.4 (a,c)) is that the interpolation and tuning scheme described in the Subsection 2.2 already contains this effect by using the tuned values for Pu_{av}. Note that it is assumed that both α_{S1} and α_{S2} are independent of sideslip angle. This was done to keep the model simple, but could be easily incorporated if needed. A value of 4° for α_{S1} was extracted from the test data for zero sideslip angle, using the criterion of negative curvature of the lift coefficient. A value of 12° was used for α_{S2} as this was found to provide good correlation between the interpolated model and test results.

The forces and moments for the lateral plane use the same structure as equations (A.1)-(A.4), with angle-of-attack (α) replaced by the drift angle (γ), the subscript x replaced by y, and pitch moment coefficient CM replaced by roll moment coefficient CR (note that for CR calculation, fin span should be used as a reference length in place of fin chord). The non-dimensional lateral forces and moments coefficients are given as:

$$\begin{aligned}
&\text{(a)}\quad C_y = -\frac{V_{yz}^{\,2}}{V_\infty^{\,2}}\left(-C_L \mathrm{Sin}|\gamma| + C_D \mathrm{Cos}|\gamma|\right)\cdot \mathrm{Sign}(v)\\
&\text{(b)}\quad C_{z_{yz}} = -C_{n_{yz}}\cdot \mathrm{Sign}(w)\\
&\text{(c)}\quad C_{M_x} = \frac{V_{yz}^{\,2}}{V_\infty^{\,2}} C_R \cdot \mathrm{Sign}(v\cdot w)
\end{aligned} \qquad \ldots (A.5)$$

For the specific fin used, it was assumed that the effects caused by the fin roll moment and spanwise shift in the centre of pressure (y_{cp}) can be neglected. Thus, $C_R(\alpha,\beta)$ is assumed equal to zero, and y_{cp} is assumed to be constantly fixed at 0·5 (mid span). The justification for these assumptions stems from the observation that the anticipated fins sideslip angle that would be encountered during slung load carriage are not close to ±90°, hence the expected contribution of the above to the net aerodynamic moments should be small to negligible (note that due to fin orientation relative to the load, the definition of fin sideslip angle is entirely different from the load sideslip angle).

APPENDIX B: LOAD EQUATIONS OF MOTION

Defining the load's inertial velocity and angular rate vectors as $\underline{\mathbf{V}}$ and $\underline{\boldsymbol{\omega}}$, respectively, the load six degrees of freedom equations are:

$$\begin{aligned}
\left[\underline{\underline{I}} + m\cdot\left(\underline{r}\right)^{\otimes}\cdot\left(\underline{r}\right)^{\otimes}\right]\dot{\underline{\omega}} = \left(\underline{H}\right)^{\otimes}\cdot\underline{\omega} - m\cdot\left(\underline{r}\right)^{\otimes}\cdot\left(\underline{\omega}\right)^{\otimes}\cdot\left(\underline{\omega}\right)^{\otimes}\cdot\underline{r} - m\cdot\left(\underline{r}\right)^{\otimes}\cdot D_W^L\cdot\underline{g} + \\
+ q_\infty S_{REF}\left(l_{REF}\cdot\underline{C}_M - \left(\underline{r}\right)^{\otimes}\cdot\underline{C}_F\right)
\end{aligned} \qquad \ldots (B.1)$$

$$\dot{\underline{V}} = \left(\underline{r}\right)^{\otimes}\cdot\dot{\underline{\omega}} \qquad \ldots (B.2)$$

In these equations m and $\underline{\underline{I}}$ are the load mass and inertia tensor, $\underline{r}$ is the load's cg vector measured from the slings to gimbal attachment point, $\underline{H}$ is the load angular momentum given by $\underline{\underline{I}}\cdot\underline{\omega}$, while $\underline{C}_F$ and $\underline{C}_M$ are the load aerodynamic forces and moments coefficients. D_W^L is the Euler transformation matrix from wind tunnel axes to load fixed axes, and $\mathbf{g}$ is the gravity acceleration vector in wind tunnel axes. The symbol $(\ )^{\otimes}$ denotes the skew-symmetric matrix of a vector, which allows the representation of a vector cross products as a matrix multiplication.

https://doi.org/10.1017/S0001924000011143 Published online by Cambridge University Press

A supplemental set of equations relate the load's angular rate to the Euler angles rate of change:

$$\begin{pmatrix} \dot{\psi} \\ \dot{\theta} \\ \dot{\phi} \end{pmatrix} = \begin{pmatrix} 0 & \frac{\mathrm{Sin}\phi}{\mathrm{Cos}\theta} & \frac{\mathrm{Cos}\phi}{\mathrm{Cos}\theta} \\ 0 & \mathrm{Cos}\phi & -\mathrm{Sin}\phi \\ 1 & \mathrm{Sin}\phi\mathrm{Tan}\theta & \mathrm{Cos}\phi\mathrm{Tan}\theta \end{pmatrix} \cdot \underline{\omega} \qquad \ldots (B.3)$$

This first order system of ordinary differential equations is solved for a certain set of initial conditions, using numerical integration to provide the load dynamic parameters time histories: $\underline{V}(t)$, $\underline{\omega}(t)$, $\psi(t)$, $\theta(t)$, $\phi(t)$.

https://doi.org/10.1017/S0001924000011143 Published online by Cambridge University Press